

# Superresolution in Interferometric Imaging of Strong Thermal Sources

Yunkai Wang,<sup>1,2</sup> Yujie Zhang,<sup>1,2</sup> and Virginia O. Lorenz<sup>1,2,\*</sup>

<sup>1</sup>*IQUIST, University of Illinois at Urbana-Champaign, Urbana, IL 61801 USA*

<sup>2</sup>*Department of Physics, University of Illinois at Urbana-Champaign, Urbana, IL 61801 USA*

(Dated: January 27, 2021)

Imaging using interferometer arrays based on the Van Cittert-Zernike theorem has been widely used in astronomical observation. Recently it was shown that superresolution can be achieved in this system for imaging two weak thermal point sources. Using quantum estimation theory, we consider the fundamental quantum limit of resolving the transverse separation of two strong thermal point sources using interferometer arrays, and show that the resolution is not limited by the longest baseline. We propose measurement techniques using linear beam splitters and photon-number-resolving detection to achieve our bound. Our results demonstrate that superresolution for resolving two thermal point sources of any strength can be achieved in interferometer arrays.

*Introduction-* Rayleigh's limit, which says that with a single lens imaging system we cannot resolve sources with separation less than the diffraction-limited spot size of the point spread function, has been widely used to quantify imaging resolution [1]. Rayleigh's limit was revisited from the perspective of quantum metrology by Tsang *et al.* [2], who showed that Rayleigh's limit of estimating the separation of two weak incoherent point sources using a single lens can be overcome with more carefully designed measurement strategies. From the quantum metrology perspective, Rayleigh's limit is a consequence of an improperly chosen measurement that both restricts access to information and destroys information by collapsing the state. A quantum mechanical description of imaging allows us to design a measurement to access information about the states through use of prior information about the source, such as the assumption of point sources of equal intensity. Since this ground-breaking result was announced, a series of studies have been conducted that expand on this result in several directions, including extending it to the case of imaging two strong thermal point sources [3, 4], estimation of point source locations in two and three dimensions [5–8], and a determination of the sensitivity limit of more general extended source imaging [9–14]. Experimentally, the quantum theory of superresolution has been verified [15, 16]. A recent review of related progress can be found in Ref. [17].

While to date superresolution theory has primarily aimed at overcoming Rayleigh's limit for a single lens system, there is another widely-used conventional imaging method based on the Van Cittert-Zernike theorem using interferometers [18]. Roughly speaking, this imaging method uses interference between signals arriving at different positions in the image plane to reconstruct the intensity distribution in the source plane. This method enables an array of telescopes to provide enhanced resolution compared to a single telescope, and has led to the thriving development of interferometric telescope arrays, especially in the radio wavelength [19, 20]. The

high angular resolution provided by the Event Horizon Telescope (EHT), a radio interferometer array, made it possible to obtain the first image of a supermassive black hole at the center of the Messier 87 Galaxy [21]. Recently, methods to improve interferometric imaging systems using quantum information techniques have been proposed that show transmission loss between two nodes in an optical interferometric array can be circumvented by quantum networks [22, 23]. The precision with which the mutual coherence can be measured has also been explored both theoretically and experimentally using quantum estimation theory [24, 25]. It is well-known that the ability to resolve two point sources using interferometric telescope arrays based on the Van Cittert-Zernike theorem is limited by the longest baseline (we provide a detailed introduction to the resolution limit of interferometer arrays in Appendix A). This resolution limit also holds even for the methods that improve the sensitivity of estimating the coherence function in Refs. [22–25]. The reason behind this resolution limit is the incomplete sampling of the image plane, which is similar to Rayleigh's limit with finite aperture size. Given these facts, it is then very tempting to ask whether one can achieve superresolution for interferometric imaging systems.

One affirmative answer to this question has recently been given in Ref. [14]. They consider an arbitrary number of weak incoherent thermal point sources observed by a system of collectors and determine the fundamental limit of sensing the parameters related to the position of the sources. Their result shows that in the ideal case, there is no resolution limit for estimating the separation between two weak point sources using interferometric telescope arrays. However, the case of arbitrary intensity needs to be checked, because multiphoton coincidences and photon bunching, which have been ignored [14], have significant effects in some situations [26]. In this work, using quantum estimation theory we show that superresolution can be achieved for thermal sources of arbitrary strength. We show the optimal measurement strategy can be implemented using linear beam splitters and photon-number-resolving detection. Although our discussion arises from imaging in astronomy, these results

---

\*Electronic address: vlorenz@illinois.edu

are applicable to any general far-field imaging problem.

### Theoretical Model

We model the quantum state received from two strong thermal point sources of equal intensity by a linear interferometer with two telescopes in the paraxial regime. We assume the positions of the two point sources can be described in one dimension as  $X_1$  and  $X_2$ , as shown in Fig. 1. The two point sources are assumed to be monochromatic and can be described by the canonical annihilation and creation operators  $c_1$ ,  $c_1^\dagger$  and  $c_2$ ,  $c_2^\dagger$ . The two modes  $a_1$ ,  $a_1^\dagger$  and  $a_2$ ,  $a_2^\dagger$  of the interferometer in the image plane receive the state from the sources with phases  $\phi_1$  and  $\phi_2$  due to the difference in light path length, which contains information on the position of the sources. We explicitly derive the relation between  $\phi_1$ ,  $\phi_2$  and the parameters of the settings (detailed in Appendix B) as

$$\phi_i = kB \frac{X_i}{s_0}, \quad i = 1, 2, \quad (1)$$

where  $B$  is the length of the baseline,  $k$  is the wavevector of the light and  $s_0$  is the longitudinal distance to the source plane.

Similar to the derivation in Ref. [3], the states received in the interferometer modes  $a_1$  and  $a_2$  are an attenuated version of the source modes  $c_1$  and  $c_2$ ,

$$c_i \rightarrow \sqrt{\eta}a_1 + \sqrt{\eta}e^{i\phi_i}a_2 + \sqrt{1-2\eta}v_i, \quad i = 1, 2, \quad (2)$$

where  $v_i$  are auxiliary environmental modes and  $\eta$  is the attenuation ratio. Starting from the thermal states of the source  $c_1$  and  $c_2$ , we derive the states received by the interferometer (detailed in Appendix C) as

$$\begin{aligned} \rho = & \frac{1}{(\pi\eta\bar{N})^2} \int_{C^2} d^2\alpha_1 d^2\alpha_2 \exp\left(-\frac{|\alpha_1|^2 + |\alpha_2|^2}{\eta\bar{N}}\right) \\ & \times [|\alpha_1 + \alpha_2\rangle \langle \alpha_1 + \alpha_2| \\ & \otimes |\alpha_1 e^{-i\phi_1} + \alpha_2 e^{-i\phi_2}\rangle \langle \alpha_1 e^{-i\phi_1} + \alpha_2 e^{-i\phi_2}|], \end{aligned} \quad (3)$$

where  $\bar{N}$  represents the strength of each source and  $|\alpha_1 + \alpha_2\rangle$  and  $|\alpha_1 e^{-i\phi_1} + \alpha_2 e^{-i\phi_2}\rangle$  are the coherent states of the two interferometer modes  $a_1$  and  $a_2$ . We have confirmed the derived state is still a Gaussian state in Appendix C. Gaussian states are completely characterized by their mean displacement  $\lambda_\mu = \text{Tr}[\rho \mathbf{a}_\mu]$ , where  $\mathbf{a} = [a_1, a_1^\dagger, a_2, a_2^\dagger]$ , and covariance matrix  $\Sigma_{\mu\nu} = \frac{1}{2} \text{Tr}[\rho(\tilde{\mathbf{a}}_\mu \tilde{\mathbf{a}}_\nu + \tilde{\mathbf{a}}_\nu \tilde{\mathbf{a}}_\mu)]$ , with  $\tilde{\mathbf{a}}_\mu = \mathbf{a}_\mu - \lambda_\mu$  [27, 28]. The mean displacement  $\lambda_\mu$  and covariance matrix  $\Sigma$  of  $\rho$  are given by

$$\begin{aligned} \lambda_\mu &= 0, \quad \text{for } \forall \mu, \\ \Sigma &= \begin{bmatrix} 0 & p & 0 & q \\ p & 0 & q^* & 0 \\ 0 & q^* & 0 & p \\ q & 0 & p & 0 \end{bmatrix}, \end{aligned} \quad (4)$$

where  $p = 2\eta\bar{N} + \frac{1}{2}$  and  $q = (e^{i\phi_1} + e^{i\phi_2})\eta\bar{N}$ .

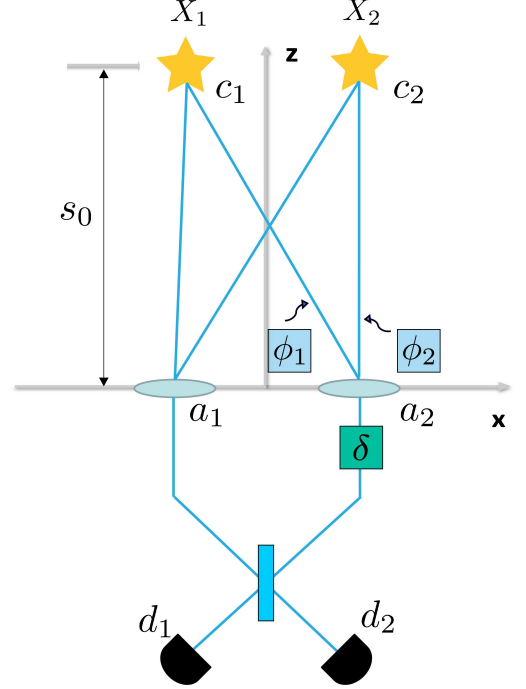


Figure 1: Schematic of setup for estimating the position of two strong thermal point sources  $c_1$  and  $c_2$  at positions  $X_1$  and  $X_2$ , respectively. The light from the two sources are collected with a two-mode interferometer. States received by the two interferometer modes differ by the phases  $\phi_1$  and  $\phi_2$  due to the difference in path length.

### Fundamental Sensitivity Limit

We now consider the fundamental limit of resolving two point sources with two telescopes. For two point sources, the resolution is reflected in the sensitivity of measuring the centroid  $\theta_1 = \frac{1}{2}(X_1 + X_2)$  and the separation between the two sources  $\theta_2 = X_1 - X_2$ . The sensitivity of estimating  $\theta_1$  and  $\theta_2$  is bounded by the quantum Fisher information  $F$ :  $\Sigma_{\tilde{\theta}} \geq F^{-1}$ , with its  $(\mu, \nu)$  element  $[\Sigma_{\tilde{\theta}}]_{\mu\nu} = \mathbb{E}[(\theta_\mu - \tilde{\theta}_\mu)(\theta_\nu - \tilde{\theta}_\nu)]$ , where  $\tilde{\theta}_\mu$  is the unbiased estimator of the  $\mu$ -th unknown parameter. This sensitivity limit is the quantum Cramér-Rao bound (QCRB). The matrix element  $F_{ij}$  of the QFI of a Gaussian state has been derived as a closed form expression in terms of  $\lambda_\mu$  and  $\Sigma$  in Ref. [29]:

$$F_{ij} = \frac{1}{2} \mathfrak{M}_{\alpha\beta, \mu\nu}^{-1} \partial_j \Sigma_{\alpha\beta} \partial_i \Sigma_{\mu\nu} + \Sigma_{\mu\nu}^{-1} \partial_j \lambda_\mu \partial_i \lambda_\nu, \quad (5)$$

where  $\mathfrak{M} = \Sigma \otimes \Sigma + \frac{1}{4} \Omega \otimes \Omega$ , with  $\Omega = \bigoplus_{k=1}^n i\sigma_y$  with  $\sigma_y$  being the Pauli  $y$  matrix,  $\partial_j$  is the derivative over the  $j$ -th unknown parameter, and repeated indices imply summation.

The quantum Fisher information for the separation  $\theta_2$  is then given by

$$F_{22} = -\frac{k^2 B^2}{s_0^2} \frac{\eta \bar{N}(1 + 3\eta \bar{N} + \eta \bar{N} \cos(\phi_1 - \phi_2))}{-1 - 2\eta \bar{N}(2 + \eta \bar{N}) + 2\eta^2 \bar{N}^2 \cos(\phi_1 - \phi_2)} \xrightarrow{\theta_2 \rightarrow 0} \frac{k^2 B^2}{s_0^2} \eta \bar{N}. \quad (6)$$

We emphasize that when the separation between the two point sources tends to zero, i.e.  $\theta_2 \rightarrow 0$ , the quantum Fisher information tends to a constant. This implies that there is actually no resolution limit for resolving two strong thermal point sources. Furthermore, we have checked that the QFI is diagonalized, i.e.  $F_{12} = F_{21} = 0$ , and hence it is possible to measure the separation and the centroid independently. The quantum Fisher information  $F_{11}$  for estimating the centroid,  $\theta_1$ , also tends to a constant as the separation  $\theta_2 \rightarrow 0$ , as detailed in Appendix D; we discuss this result after analyzing the QFI for the separation. We plot the values of  $F_{22}$  as a function of the separation  $\theta_2$  for different source strengths  $\bar{N}$  in Fig. 2. The QFI shows periodicity over  $\theta_2$  with period  $2\pi s_0/(kB)$ , which is roughly the conventional resolution limit of interferometry. We observe that for the intermediate values of  $\theta_2$  within a period, the QFI decreases with increasing source strength  $\bar{N}$ ; this is in contrast to the limit of a weak thermal source, in which the QFI is a constant versus separation  $\theta_2$  [14]. As pointed out by Ref. [4] in the single lens case, this is a net result of multiphoton events. Note that Fig. 2 is a plot of the QFI *per photon*, which decreases for some values of  $\theta_2$  as source strength increases, but a stronger source still has a larger total QFI of estimating  $\theta_2$  given its larger photon number. We have verified this and found  $\partial F_{22}/\partial(\eta \bar{N})$  is always positive for all possible parameters.

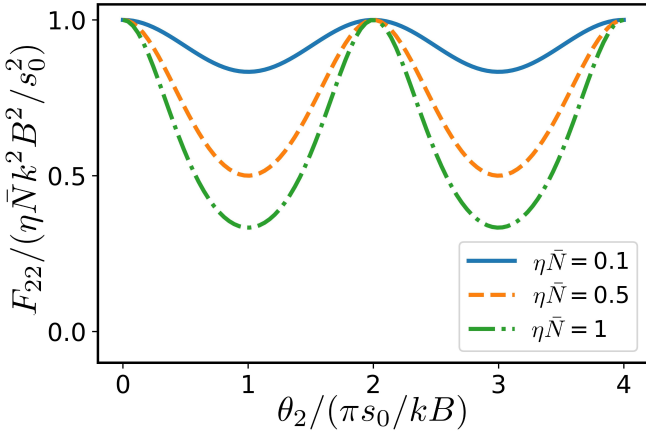


Figure 2: The quantum Fisher information  $F_{22}$  for estimating the separation, in units of  $\eta \bar{N} k^2 B^2 / s_0^2$ , as a function of the separation  $\theta_2$ , for different source strengths  $\bar{N}$ .

We now consider what the proper measurement strategy is to actually achieve this limit. The positive

operator-valued measure (POVM) that can saturate the QCRB is given by the eigenbasis of the symmetric logarithmic derivative (SLD) [30]. For a Gaussian state, the SLD has been derived in terms of its mean displacement  $\lambda_\mu$  and covariance matrix  $\Sigma$  [29]:

$$\mathcal{L}_i = \frac{1}{2} \mathfrak{M}_{\gamma\kappa, \alpha\beta}^{-1} (\partial_i \Sigma_{\alpha\beta}) (a_\gamma a_\kappa - \Sigma_{\gamma\kappa}), \quad (7)$$

where  $a_i$  is the mode operator and we sum over repeated indices. The SLD for estimating the separation  $\theta_2$  is:

$$\mathcal{L}_{\theta_2} = 2l_1 a_1^\dagger a_1 + 2l_1 a_2^\dagger a_2 + 2l_2 a_1 a_2^\dagger + 2l_2^* a_1^\dagger a_2 + C_{\theta_2}, \quad (8)$$

where

$$\begin{aligned} C_{\theta_2} &= -\eta \bar{N} [8l_1 + 2l_2 (e^{i\phi_1} + e^{i\phi_2}) + 2l_2^* (e^{-i\phi_1} + e^{-i\phi_2})], \\ l_1 &= \frac{kB}{s_0} \frac{(1 + 4\eta \bar{N}) \cot \frac{\phi_1 - \phi_2}{2}}{-4[1 + 2\eta \bar{N}(2 + \eta \bar{N})] + 8\eta^2 \bar{N}^2 \cos(\phi_1 - \phi_2)}, \\ l_2 &= -\frac{kB}{s_0} \times \frac{e^{-\frac{1}{2}i(\phi_1 + \phi_2)} (1 + 3\eta \bar{N} + \eta \bar{N} \cos(\phi_1 - \phi_2)) \csc \frac{\phi_1 - \phi_2}{2}}{4[-1 - 2\eta \bar{N}(2 + \eta \bar{N}) + 2\eta^2 \bar{N}^2 \cos(\phi_1 - \phi_2)]}. \end{aligned} \quad (9)$$

To find the eigenbasis of the SLD, we diagonalize  $\mathcal{L}_{\theta_2}$ . Assuming  $d_1 = \frac{1}{\sqrt{2}}(a_1 + e^{i\delta} a_2)$ ,  $d_2 = \frac{1}{\sqrt{2}}(a_1 - e^{i\delta} a_2)$  and dropping the constant terms, we have

$$\begin{aligned} \mathcal{L}_{\theta_2} &= (2l_1 + l_2 e^{i\delta} + l_2^* e^{-i\delta}) d_1^\dagger d_1 \\ &\quad + (2l_1 - l_2 e^{i\delta} - l_2^* e^{-i\delta}) d_2^\dagger d_2 \\ &\quad + (l_2 e^{i\delta} - l_2^* e^{-i\delta}) d_1^\dagger d_2 - (l_2 e^{i\delta} - l_2^* e^{-i\delta}) d_2^\dagger d_1. \end{aligned} \quad (10)$$

We can choose  $l_2 e^{i\delta} - l_2^* e^{-i\delta} = 0$  or equivalently  $\delta = \frac{1}{2}(\phi_1 + \phi_2)$ , which means the SLD has the Fock basis of  $d_1, d_2$  as its eigenbasis. Thus, the optimal POVM for estimating  $\theta_2$  is  $\{|m, n\rangle \langle m, n|\}_{m,n}$ , with  $d_1^\dagger d_1 |m, n\rangle = m |m, n\rangle$  and  $d_2^\dagger d_2 |m, n\rangle = n |m, n\rangle$ .

As shown in Fig. 1, we can implement the above POVM by combining the states of the two modes of the two telescopes on a beam splitter, adding a fixed phase delay  $\delta$  corresponding to the optimal delay found above to one of the arms, and performing photon-number-resolved detection in both of the two output ports. This setup is the same as found in Ref. [14], except for the photon-number-resolved detection. More specifically, for the weak thermal source discussed in Ref. [14] and in Appendix E, the quantum state  $\rho$  received by the two telescopes in modes  $a_1$  and  $a_2$  is in a Hilbert space spanned by the Fock state basis  $\{|m, n\rangle\}$  with constraint  $m+n \leq 1$  – no such constraint is present for the case of a strong thermal source. In order to implement the POVM found above, the state is measured for each temporal mode and projected onto one of the Fock bases  $|m, n\rangle$ . Data is accumulated to find the probability  $P(m, n)$  of getting each outcome. The probability distribution is then fit with

its corresponding theoretical prediction to obtain the unknown centroid or separation. The theoretical prediction for the first few  $P(m, n)$  is given in Fig. 3. The probability distribution  $P(m, n)$  is symmetric with respect to  $\phi_2 - \phi_1 = 2\pi$  as a function of  $\phi_2 - \phi_1$ , so for some separations there exists ambiguity in the estimation – this is resolved through measurement of the centroid  $\theta_1 \propto \phi_1 + \phi_2$ , discussed below. In practice, the detectors may be able to distinguish only the first few Fock states of low photon number. As shown in Fig. 4, even if only Fock states  $|m, n\rangle$  with  $m \leq M, n \leq N$  can be distinguished, the FI still maintains a reasonable amount of the QFI, which implies that we can achieve a large part of the sensitivity predicted in the ideal case. In particular, we emphasize that even if we only distinguish the presence or absence of the photon, i.e.  $M = N = 1$ , superresolution is still achieved, as is indicated by the finite FI in this case when the separation  $\theta_2$  goes to zero.

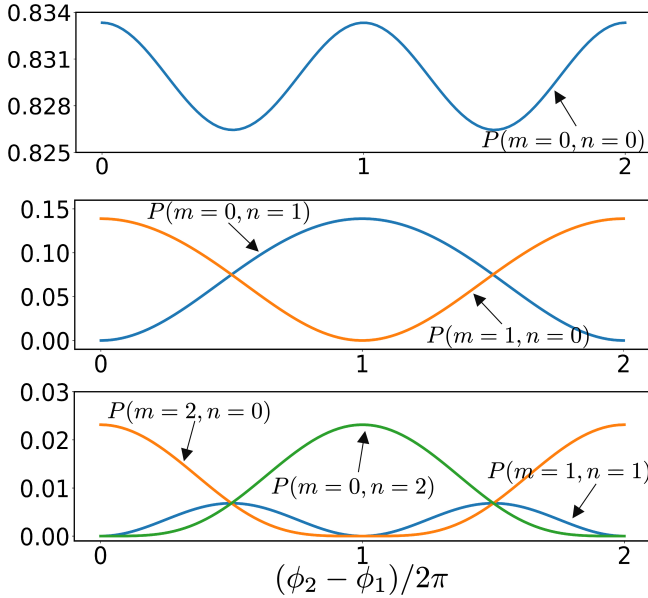


Figure 3: The probability  $P(m, n)$  of projecting the state onto  $|m, n\rangle$  with  $\eta\bar{N} = 0.1$  as a function of  $\phi_2 - \phi_1$ .

The phase delay  $\delta$  depends on the centroid  $\theta_1$  of the two point sources, since  $\theta_1 \propto \phi_1 + \phi_2$ , and thus the scheme requires accurate measurement of the centroid. The derivation for the estimation of the centroid is detailed in Appendix D; there it can be seen that a similar measurement strategy that also depends on the centroid is optimal. This recursive relationship can be overcome, as in conventional imaging there is no fundamental limitation on the accuracy of estimating the centroid; thus, other imaging methods can be used or suboptimal strategies can be constructed to determine the centroid, such as using a random phase scheme. Nevertheless, misalignment of the centroid must be taken into account. We find that, unlike superresolution using a single lens, for which any misalignment makes superresolution unachievable [2], in

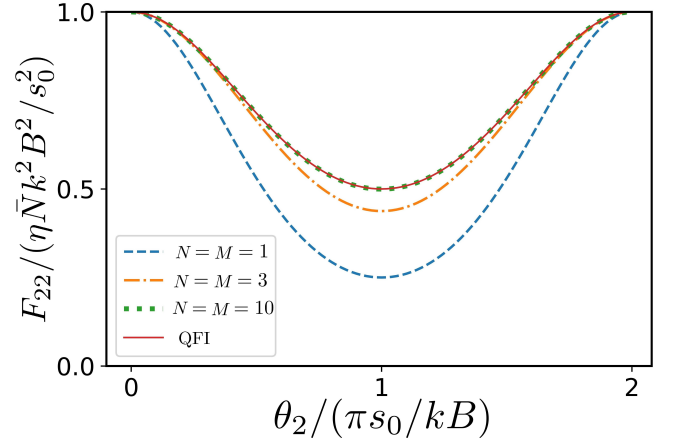


Figure 4: Fisher information for photon number detection that only distinguishes the Fock state  $|m, n\rangle$  for  $m \leq M, n \leq N$ . Events with greater photon number are ignored.

the present case, superresolution is still achievable even with some degree of misalignment. We find numerically that superresolution is no longer achieved only once the misalignment  $c = \frac{1}{2}(\phi_1 + \phi_2) - \delta$  is roughly comparable to the separation  $\theta_2$ . We discuss in detail the effect of misalignment of the centroid on the estimation of the separation in Appendix F.

We estimate the improvement our method provides compared to the conventional imaging method based on the Van Cittert-Zernike theorem using parameters similar to real present-day interferometer arrays in Appendix G. We consider the case where the observation is made with wavelength  $\lambda = 5$  mm and longest baseline  $B = 10$  km. The resolution of the conventional method is then  $\lambda/B = 5 \times 10^{-7}$  radians  $\approx 0.1''$ . When the angular separation of the two point sources is  $\theta_2/s_0 = 0.01''$  and  $\eta\bar{N} = 0.01$ , the Fisher information of our optimal measurement is larger than the conventional method by a factor of roughly 30. If we assume the mean square error of estimating the angular separation  $\theta_2/s_0$  scales with the number of samples  $n$  as  $\Delta(\theta_2/s_0)^2 \propto 1/n$ , this implies that our optimal measurement can shorten the observation time by a factor of 30 to achieve the same sensitivity.

*Conclusion-* In summary, we have used quantum estimation theory to determine the fundamental limit of resolving two identical thermal point sources of any strength. The results show that, unlike the conventional imaging method based on the Van Cittert-Zernike theorem, a more properly designed measurement scheme can achieve a resolution not limited by the longest baseline. We find a measurement scheme using a beam splitter and photon-number-resolving detection can achieve the resolution given by the quantum Cramér-Rao bound. This work can be extended to several other cases, such as resolving two point sources with large intensity difference, estimating separation in 3 dimensions, and imaging a



general extended source. We hope our result inspires more discussion along these lines.

## I. ACKNOWLEDGEMENTS

We thank Offir Cohen, Andrew Jordan, Brian Smith and Jing Yang for helpful discussion. This work was sup-

ported by the multi-university National Science Foundation Grant No. 193632 – QII-TAQS: Quantum-Enhanced Telescopy.

- 
- [1] L. Rayleigh, Investigations in optics, with special reference to the spectroscope, *Philos. Mag. J. Sci* **8**, 261 (1879).
  - [2] M. Tsang, R. Nair, and X.-M. Lu, Quantum theory of superresolution for two incoherent optical point sources, *Phys. Rev. X* **6**, 031033 (2016).
  - [3] C. Lupo, and S. Pirandola, Ultimate precision bound of quantum and subwavelength imaging, *Phys. Rev. Lett.* **117**, 190802 (2016).
  - [4] R. Nair, and M. Tsang, Far-field superresolution of thermal electromagnetic sources at the quantum limit, *Phys. Rev. Lett.* **117**, 190801 (2016).
  - [5] S. Z. Ang, R. Nair, and M. Tsang, Quantum limit for two-dimensional resolution of two incoherent optical point sources, *Phys. Rev. A* **95**, 063847 (2017).
  - [6] Z. Yu, and S. Prasad, Quantum limited superresolution of an incoherent source pair in three dimensions, *Phys. Rev. Lett.* **121**, 180504 (2018).
  - [7] C. Napoli, S. Piano, R. Leach, G. Adesso, and T. Tufarelli, Towards superresolution surface metrology: Quantum estimation of angular and axial separations, *Phys. Rev. Lett.* **122**, 140505 (2019).
  - [8] S. Prasad, and Z. Yu, Quantum-limited superlocalization and superresolution of a source pair in three dimensions, *Phys. Rev. A* **99**, 022116 (2019).
  - [9] Z. Dutton, R. Kerviche, A. Ashok, and S. Guha, Attaining the quantum limit of superresolution in imaging an object's length via predetection spatial-mode sorting, *Phys. Rev. A* **99**, 033847 (2019).
  - [10] S. Zhou, and L. Jiang, Modern description of rayleigh's criterion, *Phys. Rev. A* **99**, 013808 (2019).
  - [11] M. Tsang, Quantum limit to subdiffraction incoherent optical imaging, *Phys. Rev. A* **99**, 012305 (2019).
  - [12] M. Tsang, Semiparametric estimation for incoherent optical imaging, *Phys. Rev. Research* **1**, 033006 (2019).
  - [13] M. Tsang, F. Albarelli, and A. Datta, Quantum semiparametric estimation, *Phys. Rev. X* **10**, 031023 (2020).
  - [14] C. Lupo, Z. Huang, and P. Kok, Quantum limits to incoherent imaging are achieved by linear interferometry, *Phys. Rev. Lett.* **124**, 080503 (2020).
  - [15] Y. Zhou, *et al.* Quantum-limited estimation of the axial separation of two incoherent point sources, *Optica* **6**, 534 (2019).
  - [16] W.-K. Tham, H. Ferretti, and A. M. Steinberg, Beating rayleigh's curse by imaging using phase information, *Phys. Rev. Lett.* **118**, 070801 (2017).
  - [17] M. Tsang, Resolving starlight: a quantum perspective, *Contemp. Phys.* **60**, 279 (2019).
  - [18] F. Zernike, The concept of degree of coherence and its application to optical problems, *Physica* **5**, 785 (1938).
  - [19] T. L. Wilson, K. Rohlf, and S. Hüttemeister, *Tools of radio astronomy*, (Springer, Berlin, 2009).
  - [20] K. Kellermann, and J. Moran, The development of high-resolution imaging in radio astronomy, *Annu. Rev. Astron. Astrophys.* **39**, 457 (2001).
  - [21] Event Horizon Telescope Collaboration *et al.*, First m87 event horizon telescope results. i. the shadow of the supermassive black hole, *Astrophys. J. Lett.* **875**, L1 (2019).
  - [22] D. Gottesman, T. Jennewein, and S. Croke, Longer-baseline telescopes using quantum repeaters, *Phys. Rev. Lett.* **109**, 070503 (2012).
  - [23] E. T. Khabiboulline, J. Borregaard, K. De Greve, and M. D. Lukin, Optical interferometry with quantum networks, *Phys. Rev. Lett.* **123**, 070504 (2019).
  - [24] M. E. Pearce, E. T. Campbell, and P. Kok, Optimal quantum metrology of distant black bodies, *Quantum* **1**, 21 (2017).
  - [25] L. A. Howard, G. G. Gillett, M. E. Pearce, R. A. Abraham, T. J. Weinhold, P. Kok, and A. G. White, Optimal imaging of remote bodies using quantum detectors, *Phys. Rev. Lett.* **123**, 143604 (2019).
  - [26] L. Mandel, and E. Wolf, *Optical coherence and quantum optics*, (Cambridge University Press, 1995).
  - [27] S. Braunstein, and P. van Loock, Quantum information with continuous variables, *Rev. Mod. Phys.* **77**, 513 (2005).
  - [28] C. Weedbrook, S. Pirandola, R. García-Patrón, N. J. Cerf, T. C. Ralph, J. H. Shapiro, and S. Lloyd, Gaussian quantum information, *Rev. Mod. Phys.* **84**, 621 (2012).
  - [29] Y. Gao, and H. Lee, Bounds on quantum multiple-parameter estimation with gaussian state, *Eur. Phys. J. D* **68**, 347 (2014).
  - [30] M. G. Paris, Quantum estimation for quantum technology, *Int. J. Quantum. Inform.* **7**, 125–137 (2009).
  - [31] M. Tsang, Quantum nonlocality in weak-thermal-light interferometry, *Phys. Rev. Lett.* **107**, 270402 (2011).

## Appendix A: Resolution limit of the conventional method

Here we briefly review the resolution limit of the conventional imaging method based on the Van Cittert-Zernike theorem. We refer the reader to Ref. [19, 20] for more details. The Van Cittert-Zernike theorem relies on the fact that the mutual coherence function of the signal  $V(u, v)$  between two points on the image plane is the Fourier transformation of the intensity distribution  $I(l, m)$  in the source plane:

$$V(u, v) = \iint I(l, m) \exp[2\pi i(lu + mv)] dl dm, \quad (\text{A1})$$

where  $(u, v)$  are the coordinates of the baseline between the two observation points in the image plane, and  $(l, m)$  are the coordinates of one point in the source plane. Of course, if we could measure all the Fourier components, we could completely reconstruct the intensity distribution, i.e. the image, with no resolution limit. But this requires us to measure the entire function  $V(u, v)$ , with each point of this function obtained by a measurement with particular baseline  $\vec{B} = (u, v)$ , which is practically impossible.

We now determine the resolution for a finite number of samples of the image plane. We first introduce a sampling function  $S(u, v)$  that takes value  $S(u, v) = 1$  at the points we measure and takes value  $S(u, v) = 0$  where we do not measure, for simplicity. We then define its Fourier transformation  $B(l, m) = FT\{S(u, v)\}$ , where  $FT\{\cdot\}$  means Fourier transformation; this is similar to the point spread function in the single lens imaging method, usually called the dirty beam. Performing an inverse Fourier transformation on the measured coherence function gives  $I^D(l, m) = FT\{V(u, v)S(u, v)\} = I'(l, m) * B(l, m)$ , where  $*$  means convolution and  $I'(l, m) = FT\{V(u, v)\}$  is the actual intensity distribution;  $I^D(l, m)$  is usually called the dirty image. Mathematically, it is not possible to take the inverse of the convolution. In astronomical observation, a de-convolution method is carefully designed to gain some information from the dirty image, but as the convolution is not invertible, these empirical methods rely on some assumptions and provide limited resolution that depends on the length of the baseline. We could say the resolution is limited by the dirty beam  $B(l, m)$  in this method, which is very similar to the resolution limit of conventional imaging systems with a single lens, where the point spread function causes the limitation due to the finite size of the aperture.

As a simple example, consider the sampling function  $S(u, v) = 1$  if  $-d \leq u \leq d$  and  $-d \leq v \leq d$  and  $S(u, v) = 0$  everywhere else, which means the longest baseline is  $d$ . Then the dirty beam is  $B(l, m) = FT\{S(u, v)\} = \frac{4}{\pi^2} \frac{\sin ld}{l} \frac{\sin md}{m}$ , and the width of it in each direction is  $\pi/d$ . From this we see the resolution of the interferometer array is roughly determined by its longest baseline. Of course, a real sampling function does not have this simple form; the dirty beam has structure rather than looking like a point. A deconvolution is thus usually necessary to remove the structure introduced by the dirty beam.

We emphasize that whenever imaging is based on the Van Cittert-Zernike theorem, the resolution is limited by the effect of finite sampling. In this sense, all the discussion on improving the estimation of the coherence function in Refs. [22–25] have this resolution limit.

## Appendix B: Relation between phase and the position of the source

Here we derive the relation between the phases  $\phi_1$  and  $\phi_2$  and the positions of the sources. As shown in Fig. B1, we assume the telescopes are pointing at a point  $\vec{s}_0$  on the source plane. The relative positions of the two point sources are  $\vec{\sigma}_1 = (X_1, 0)$  and  $\vec{\sigma}_2 = (X_2, 0)$  and thus the positions of the point sources are  $\vec{s}_1 = \vec{s}_0 + \vec{\sigma}_1$  and  $\vec{s}_2 = \vec{s}_0 + \vec{\sigma}_2$ . The phase differences  $\phi_1$  and  $\phi_2$  between the light arriving from point sources  $X_1$  and  $X_2$  at the telescopes are then

$$\begin{aligned} \phi_1 &= k \frac{\vec{B} \cdot \vec{s}_1}{|\vec{s}_1|} = (kB s_0 \sin \theta + kB X_1 \cos \theta) / |\vec{s}_1|, \\ &= kB \sin \theta + kB \cos \theta \frac{X_1}{s_0} + o\left(\frac{X_1}{s_0}\right), \end{aligned} \quad (\text{B1})$$

$$\begin{aligned} \phi_2 &= k \frac{\vec{B} \cdot \vec{s}_2}{|\vec{s}_2|} = (kB s_0 \sin \theta + kB X_2 \cos \theta) / |\vec{s}_2| \\ &= kB \sin \theta + kB \cos \theta \frac{X_2}{s_0} + o\left(\frac{X_2}{s_0}\right), \end{aligned} \quad (\text{B2})$$

where we have assumed  $X_1, X_2 \ll s_0$  and expanded the phase as a series in  $\frac{X_i}{s_0}$ ; the little o notation  $o(\cdot)$  means the remaining terms are of order smaller than the terms in parentheses. In the main text, we assume the image plane is parallel to the source plane for simplicity; i.e.,  $\theta = 0$ , because a nonvanishing  $\theta$  shows no effect on the conclusion.

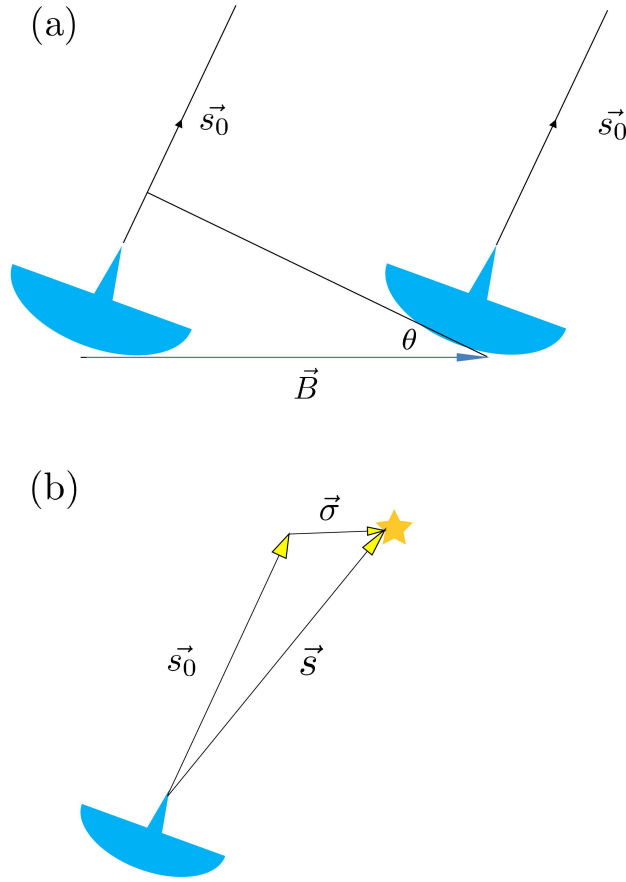


Figure B1: Diagram defining the position of the sources relative to the telescopes. (a)  $\vec{B}$  is a vector representing the baseline and  $\theta$  is the angle of the image plane relative to the source plane.  $\vec{s}_0$  is a vector connecting the observation point to the point on the source plane at which telescope is pointing. (b)  $\vec{s}$  is a point on the source and  $\vec{\sigma} = \vec{s} - \vec{s}_0$ . The phase (time) delay of signals received on the two telescopes encodes information on position.

### Appendix C: States received in modes $a_1$ and $a_2$

We assume the states emitted by the two point sources are thermal states  $\rho^{th}$  with mean photon number  $\bar{N}$ . The thermal states of two modes  $c_1$  and  $c_2$  corresponding to the two point sources are described in [28] as

$$\rho = \rho^{th}(\bar{N}) \otimes \rho^{th}(\bar{N}) = \frac{1}{(\pi\bar{N})^2} \int_{C^2} d^2\alpha_1 d^2\alpha_2 \exp\left(-\frac{|\alpha_1|^2 + |\alpha_2|^2}{\bar{N}}\right) |\alpha_1\rangle \langle\alpha_1| \otimes |\alpha_2\rangle \langle\alpha_2|, \quad (C1)$$

where  $|\alpha_1\rangle$  and  $|\alpha_2\rangle$  are the coherent states of  $c_1, c_2$ . Using the transformation from  $c_1, c_2$  to the modes of telescopes,

$$\begin{aligned} c_1 &\rightarrow \sqrt{\eta}a_1 + \sqrt{\eta}e^{i\phi_1}a_2 + \sqrt{1-2\eta}v_1, \\ c_2 &\rightarrow \sqrt{\eta}a_1 + \sqrt{\eta}e^{i\phi_2}a_2 + \sqrt{1-2\eta}v_2, \end{aligned} \quad (C2)$$

and tracing out the states of the environmental modes  $v_1$  and  $v_2$ , which we do not have access to in the measurement, we have

$$|\alpha_1\rangle \otimes |\alpha_2\rangle = D(\alpha_1)D(\alpha_2)|0\rangle \otimes |0\rangle, \quad (C3)$$

$$\begin{aligned}
D(\alpha_1)D(\alpha_2) &= \exp(\alpha_1 c_1^\dagger - \alpha_1^* c_1) \exp(\alpha_2 c_2^\dagger - \alpha_2^* c_2) \\
&= \exp\left(\frac{1}{2}\eta\alpha_1\alpha_2^* - \frac{1}{2}\eta\alpha_1^*\alpha_2\right) \exp\left(\frac{1}{2}\eta\alpha_1\alpha_2^*e^{i(\phi_2-\phi_1)} - \frac{1}{2}\eta\alpha_1^*\alpha_2e^{i(\phi_1-\phi_2)}\right) \\
&\quad \times \exp\left[\sqrt{\eta}(\alpha_1 + \alpha_2)a_1^\dagger - \sqrt{\eta}(\alpha_1^* + \alpha_2^*)a_1\right] \exp\left[\sqrt{\eta}(\alpha_1e^{-i\phi_1} + \alpha_2e^{-i\phi_2})a_2^\dagger - \sqrt{\eta}(\alpha_1^*e^{i\phi_1} + \alpha_2^*e^{i\phi_2})a_2\right].
\end{aligned} \tag{C4}$$

Hence, the state evolves to be

$$\begin{aligned}
|\alpha_1\rangle \otimes |\alpha_2\rangle &\rightarrow C |\sqrt{\eta}(\alpha_1 + \alpha_2)\rangle \otimes |\sqrt{\eta}(\alpha_1e^{-i\phi_1} + \alpha_2e^{-i\phi_2})\rangle, \\
C &= \exp\left(\frac{1}{2}\eta\alpha_1\alpha_2^* - \frac{1}{2}\eta\alpha_1^*\alpha_2\right) \exp\left(\frac{1}{2}\eta\alpha_1\alpha_2^*e^{i(\phi_2-\phi_1)} - \frac{1}{2}\eta\alpha_1^*\alpha_2e^{i(\phi_1-\phi_2)}\right).
\end{aligned} \tag{C5}$$

We then find the state received by the two modes of the two telescopes  $a_1, a_2$  as

$$\begin{aligned}
\rho &\rightarrow \frac{1}{(\pi\eta\bar{N})^2} \int_{C^2} d^2\alpha_1 d^2\alpha_2 \exp\left(-\frac{|\alpha_1|^2 + |\alpha_2|^2}{\eta\bar{N}}\right) |\alpha_1 + \alpha_2\rangle \langle \alpha_1 + \alpha_2| \\
&\quad \otimes |\alpha_1e^{-i\phi_1} + \alpha_2e^{-i\phi_2}\rangle \langle \alpha_1e^{-i\phi_1} + \alpha_2e^{-i\phi_2}|.
\end{aligned} \tag{C6}$$

We now verify the derived state of  $a_1, a_2$  above is a Gaussian state. By definition, Gaussian states written in the Wigner representation should be Gaussian, which requires the Wigner Wely operator to be:

$$\chi(\xi) := \text{tr}\left\{\rho e^{-\vec{a}^T \Omega \vec{\xi}}\right\} = \exp\left[\frac{1}{2}\vec{\xi}^T (\Omega^T \Sigma \Omega) \vec{\xi} + \vec{\xi}^T \Omega \vec{\lambda}\right], \tag{C7}$$

where  $\vec{\xi} = \{\xi_1, \xi_1^*, \xi_2, \xi_2^*\}$  and  $\Omega = -\sigma_y \otimes \sigma_y$  with  $\sigma_y$  being the Pauli  $y$  matrix.

Inserting a state of the form of Eq. 3 into the left-hand side of Eq. C7, we have:

$$\begin{aligned}
\text{Tr}\left\{\rho e^{-\vec{a}^T \Omega \vec{\xi}}\right\} &= \frac{1}{(\pi\bar{N})^2} \int_{C^2} d^2\alpha_1 d^2\alpha_2 \exp\left(-\frac{|\alpha_1|^2 + |\alpha_2|^2}{\bar{N}}\right) \exp\left(-\frac{|\xi_1|^2}{2}\right) \exp(-\sqrt{\eta}[(\alpha_1^* + \alpha_2^*)\xi_1 - (\alpha_1 + \alpha_2)\xi_1^*]) \\
&\quad \times \exp\left(-\frac{|\xi_2|^2}{2}\right) \exp(-\sqrt{\eta}[(\alpha_1^*e^{i\phi_1} + \alpha_2^*e^{i\phi_2})\xi_1 - (\alpha_1e^{-i\phi_1} + \alpha_2e^{-i\phi_2})\xi_2^*]) \\
&= \exp\left[\frac{1}{2}\vec{\xi}^T (\Omega^T \Sigma \Omega) \vec{\xi} + \vec{\xi}^T \Omega \vec{\lambda}\right],
\end{aligned} \tag{C8}$$

with  $\Sigma$  given exactly as in Eq. 4.

#### Appendix D: Estimation of the centroid

The QFI for the estimation of the centroid is given by

$$\begin{aligned}
F_{11} &= -\frac{2k^2B^2}{s_0^2} \frac{\eta\bar{N}(1 + \cos(\phi_1 - \phi_2))}{-1 - \eta\bar{N} + \eta\bar{N}\cos(\phi_1 - \phi_2)} \\
&\stackrel{\theta_2 \rightarrow 0}{=} 4 \frac{k^2B^2}{s_0^2} \eta\bar{N}.
\end{aligned} \tag{D1}$$

To find the optimal POVM that can achieve the accuracy predicted by the QCRB, we calculate the SLD for estimating the centroid  $\theta_1$  as

$$\mathcal{L}_{\theta_1} = 2l_3 a_1 a_2^\dagger + 2l_3^* a_1^\dagger a_2 + C_{\theta_1}, \tag{D2}$$



where

$$\begin{aligned} C_{\theta_1} &= -\eta\bar{N}[2l_3(e^{i\phi_1} + e^{i\phi_2}) + 2l_3^*(e^{-i\phi_1} + e^{-i\phi_2})], \\ l_3 &= i\frac{kB}{s_0} \frac{e^{-i\phi_1} + e^{-i\phi_2}}{-4 - 4\eta\bar{N} + 4\eta\bar{N}\cos(\phi_1 - \phi_2)}. \end{aligned} \quad (\text{D3})$$

To find the eigenbasis of the SLD, we diagonalize  $\mathcal{L}_{\theta_1}$ . Assuming  $d_1 = \frac{1}{\sqrt{2}}(a_1 + e^{i\delta}a_2)$ ,  $d_2 = \frac{1}{\sqrt{2}}(a_1 - e^{i\delta}a_2)$  and dropping the constant terms, we have

$$\mathcal{L}_{\theta_1} = (l_3e^{i\delta} + l_3^*e^{-i\delta})d_1^\dagger d_1 - (l_3e^{i\delta} + l_3^*e^{-i\delta})d_2^\dagger d_2 + (l_3e^{i\delta} - l_3^*e^{-i\delta})d_1^\dagger d_2 - (l_3e^{i\delta} - l_3^*e^{-i\delta})d_2^\dagger d_1. \quad (\text{D4})$$

We can choose  $l_3e^{i\delta} - l_3^*e^{-i\delta} = 0$  or equivalently  $\delta = \frac{1}{2}(\phi_1 + \phi_2) - \frac{\pi}{2}$ , which then means the SLD has the Fock basis of  $d_1, d_2$  as its eigenbasis. Thus the optimal POVM for estimating  $\theta_1$  is  $\{|m, n\rangle\langle m, n|\}_{m,n}$ , with  $d_1^\dagger d_1 |m, n\rangle = m |m, n\rangle$  and  $d_2^\dagger d_2 |m, n\rangle = n |m, n\rangle$ .

Notice the optimal POVM constructed above for the estimation of the centroid also depends on the centroid itself, so a different method would be used to measure the centroid. For example, just choosing the phase delay to be  $\delta = 0, \pi/2$  can be a method to find the centroid. Although this method is not optimal, unlike the separation, there is no fundamental limit to prevent us from improving the accuracy of estimating the centroid.

### Appendix E: Comparison with superresolution for resolving a weak thermal source

We discuss superresolution for a weak thermal source in this section, which partially overlaps with the discussion in Ref. [14]. We show that the results in the main text can be reduced to the results for weak thermal sources in the weak source limit. Similar to Ref. [31], we write down the received state from the source as

$$\begin{aligned} \rho &= (1 - \epsilon) |00\rangle\langle 00| + \frac{\epsilon}{2} [|01\rangle\langle 01| + |10\rangle\langle 10| + g^* |01\rangle\langle 10| + g |10\rangle\langle 01|] + O(\epsilon^2) \\ &= (1 - \epsilon)\rho_0 + \epsilon\rho_1 + O(\epsilon^2), \end{aligned} \quad (\text{E1})$$

where  $g = \frac{1}{2}(e^{i\phi_1} + e^{i\phi_2})$ , which encodes the information about the positions of the two sources. For a weak thermal source,  $\epsilon \ll 1$  and thus the higher order terms can be ignored; then the quantum state and the measurement POVM are on a space spanned by  $|m, n\rangle$  with  $m + n \leq 1$ .

We then diagonalize the density matrix  $\rho_1$  as

$$\rho_1 = D_1 |e_1\rangle\langle e_1| + D_2 |e_2\rangle\langle e_2|, \quad (\text{E2})$$

$$D_{1,2} = \frac{1}{2} \pm \frac{1}{4} e^{-i(\phi_1 + \phi_2)/2} (e^{i\phi_1} + e^{i\phi_2}), \quad (\text{E3})$$

$$|e_{1,2}\rangle = \pm \frac{1}{\sqrt{2}} e^{i(\phi_1 + \phi_2)/2} |01\rangle + \frac{1}{\sqrt{2}} |10\rangle. \quad (\text{E4})$$

The SLDs for both parameters  $\theta_1$  and  $\theta_2$  are then calculated as

$$\mathcal{L}_{\theta_1} = -i\frac{kB}{s_0} \cos \frac{\phi_1 - \phi_2}{2} |e_1\rangle\langle e_2| + i\frac{kB}{s_0} \cos \frac{\phi_1 - \phi_2}{2} |e_2\rangle\langle e_1|, \quad (\text{E5})$$

$$\mathcal{L}_{\theta_2} = -\frac{kB}{4D_1s_0} \sin \frac{\phi_1 - \phi_2}{2} |e_1\rangle\langle e_1| + \frac{kB}{4D_2s_0} \sin \frac{\phi_1 - \phi_2}{2} |e_2\rangle\langle e_2|. \quad (\text{E6})$$

We then calculate the QFI as

$$F = \frac{k^2 B^2}{s_0^2} \begin{bmatrix} \cos^2 \frac{\phi_1 - \phi_2}{2} & 0 \\ 0 & \frac{1}{4} \end{bmatrix}, \quad (\text{E7})$$

where  $F_{ij} = \text{Tr}(\mathcal{L}_{\theta_i} \mathcal{L}_{\theta_j} \rho)$ . It is clear that when the separation vanishes,  $\theta_2 \rightarrow 0$ , and the QFI  $F_{22}$  for estimating the separation  $\theta_2$  also remains a constant. This shows we can avoid Rayleigh's limit for observation of weak thermal

sources using interferometer arrays. The POVM to achieve the superresolution predicted by the quantum Cramer-Rao bound can be found from the eigenbasis of  $\mathcal{L}_{\theta_2}$ , which is the projective measurement  $\{|e_1\rangle\langle e_1|, |e_2\rangle\langle e_2|\}$ .

Note the implementation of the optimal POVM  $\{|e_1\rangle\langle e_1|, |e_2\rangle\langle e_2|\}$  requires us to know information about  $(\phi_1 + \phi_2)/2$ , which means we need to know the centroid of the two point sources. If the accuracy of estimating the centroid is not infinite, the sensitivity of estimating the separation is degraded; we now consider the dependence of the FI on misalignment of the centroid. Using the POVM  $\{|\tilde{e}_1\rangle\langle\tilde{e}_1|, |\tilde{e}_2\rangle\langle\tilde{e}_2|\}$ , where  $|\tilde{e}_{1,2}\rangle = \pm \frac{1}{\sqrt{2}} e^{i(\phi_1+\phi_2)/2+\delta} |01\rangle + \frac{1}{\sqrt{2}} |10\rangle$  and  $\delta$  quantifies the deviation of aligning the measurement due to the finite accuracy of knowing the centroid, the FI is degraded to be

$$I_{22} = \frac{\cos^2 \delta \sin^2 \frac{\phi_1 - \phi_2}{2}}{1 - \cos^2 \delta \cos^2 \frac{\phi_1 - \phi_2}{2}} \frac{k^2 B^2}{4s_0^2}. \quad (\text{E8})$$

If  $\delta$  is nonvanishing, when the separation  $\theta_2$  goes to zero and hence  $\phi_1 - \phi_2 \rightarrow 0$ , we find  $I_{22} \rightarrow 0$ . So just as the case for a single lens [2], the superresolution in this limit relies on the assumption that we know the centroid perfectly and align the measurement device with perfect accuracy. However, the sensitivity of estimating the separation with a limited length of baseline can be achieved by improving the estimation of the centroid and accuracy of aligning the measurement device. There is no longer a fundamental reason, such as Rayleigh's limit, that prevents us from improving the sensitivity of estimating the separation.

### Appendix F: Consequences of misalignment

In this section, we discuss the effect of misalignment in the measurement on the superresolution. We have shown in the main text that the optimal measurement that can achieve the sensitivity predicted by the quantum Cramer-Rao bound is  $\{|m, n\rangle\langle m, n|\}_{\{m, n\}}$ , with  $d_1^\dagger d_1 |m, n\rangle = m |m, n\rangle$  and  $d_2^\dagger d_2 |m, n\rangle = n |m, n\rangle$ ,  $d_1 = \frac{1}{\sqrt{2}}(a_1 + e^{i\delta} a_2)$ ,  $d_2 = \frac{1}{\sqrt{2}}(a_1 - e^{i\delta} a_2)$ ,  $\delta = \frac{1}{2}(\phi_1 + \phi_2)$ . If now  $\delta$  deviates from  $\frac{1}{2}(\phi_1 + \phi_2)$  and we write the deviation as  $c = \frac{1}{2}(\phi_1 + \phi_2) - \delta$ , the Fisher information of using  $\{|m, n\rangle\langle m, n|\}_{\{m, n\}}$  as the POVM is degraded. We now show how the superresolution predicted by the quantum Fisher information is affected by this deviation.

We first write the state  $|m, n\rangle$  using the Fock basis of mode  $a_1, a_2$ :

$$\begin{aligned} |m, n\rangle &= (d_1^\dagger)^m (d_2^\dagger)^n |0\rangle = 2^{-\frac{m+n}{2}} (a_1^\dagger + e^{-i\delta} a_2^\dagger)^m (a_1^\dagger - e^{-i\delta} a_2^\dagger)^n |0\rangle \\ &= 2^{-\frac{m+n}{2}} \sum_{j,k} C_m^j C_n^k (-1)^k e^{-i(j+k)\delta} (a_1^\dagger)^{m+n-j-k} (a_2^\dagger)^{j+k} |0\rangle, \end{aligned} \quad (\text{F1})$$

where  $C_m^j = \frac{m!}{j!(m-j)!}$ . We then evaluate

$$\begin{aligned} f(m, n, \alpha_1, \alpha_2) &= \langle m, n | (|\alpha_1 + \alpha_2\rangle \otimes |\alpha_1 e^{-i\phi_1} + \alpha_2 e^{-i\phi_2}\rangle) \\ &= 2^{-\frac{m+n}{2}} \sum_{j,k} C_m^j C_n^k (-1)^k e^{i(j+k)\delta} e^{-\frac{1}{2}|\alpha_1 + \alpha_2|^2 - \frac{1}{2}|\alpha_1 e^{-i\phi_1} + \alpha_2 e^{-i\phi_2}|^2} (\alpha_1 + \alpha_2)^{m+n-j-k} (\alpha_1 e^{-i\phi_1} + \alpha_2 e^{-i\phi_2})^{j+k}. \end{aligned} \quad (\text{F2})$$

The probability of getting outcome  $|m, n\rangle\langle m, n|$  is given by

$$P(m, n) = \frac{1}{(\pi\bar{N})^2} \int_{C^2} d^2\alpha_1 d^2\alpha_2 \exp\left(-\frac{|\alpha_1|^2 + |\alpha_2|^2}{\bar{N}}\right) |f(m, n, \alpha_1, \alpha_2)|^2. \quad (\text{F3})$$

The Fisher information of estimating the separation is calculated as

$$FI = \sum_{m,n=0}^{\infty} \frac{(\partial P(m, n)/\partial \theta_2)^2}{P(m, n)}. \quad (\text{F4})$$

This calculation is intractable both numerically and analytically. We instead make the following approximation. First, we only keep the contribution of  $|m, n\rangle\langle m, n|$  with  $m \leq 3, n \leq 3$ . As pointed out in the main text, keeping only the first few elements of the POVM can still achieve superresolution; i.e., the Fisher information tends to a constant when the separation  $\theta_2 \rightarrow 0$ . Secondly, we do the integration for the phase and amplitude of  $\alpha_1, \alpha_2$  separately and define a cut-off for the integration of the amplitude:

$$P(m, n) \approx \frac{1}{(\pi\bar{N})^2} \int_0^b d|\alpha_1| \int_0^b d|\alpha_2| \exp\left(-\frac{|\alpha_1|^2 + |\alpha_2|^2}{\bar{N}}\right) |\alpha_1||\alpha_2| g(m, n, |\alpha_1|, |\alpha_2|), \quad (\text{F5})$$

$$g(m, n, |\alpha_1|, |\alpha_2|) = \int_0^{2\pi} d\beta_1 \int_0^{2\pi} d\beta_2 |f(m, n, |\alpha_1|e^{i\beta_1}, |\alpha_2|e^{i\beta_2})|^2, \quad (\text{F6})$$

where  $\alpha_1 = |\alpha_1|e^{i\beta_1}$ ,  $\alpha_2 = |\alpha_2|e^{i\beta_2}$ , and  $b$  is a finite number. For a fixed value of  $\bar{N}$ , the FI tends to a constant value as  $b$  increases, as shown in Fig. F2(a).

We plot the FI as a function of separation  $\theta_2$  with fixed misalignment  $c$  in Fig. F2(b). It is clear that when the separation tends to zero, with a nonzero misalignment the FI vanishes and superresolution cannot be achieved. We also plot the FI as a function of the misalignment  $c$  with fixed separation  $\theta_2$  in Fig. F2(c). We observe that increasing the misalignment significantly degrades the FI. The threshold is roughly  $c \approx \theta_2$  from the figure.

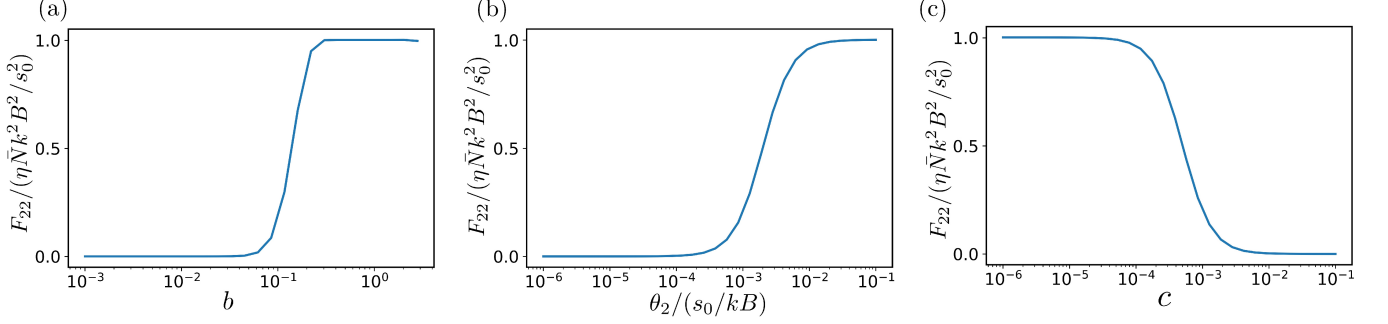


Figure F2: (a) Approximate Fisher information as a function of the integration range  $[0, b]$ . Other parameters are chosen as  $\bar{N} = 0.01$ ,  $m, n \leq 3$ ,  $c = 10^{-6}$ ,  $\theta_2 = 10^{-3}$ . (b) Approximate Fisher information as a function of separation  $\theta_2$  for fixed misalignment  $c = 10^{-3}$ . Other parameters are chosen as  $\bar{N} = 0.01$ ,  $m, n \leq 3$ . (c) Approximate Fisher information as a function of misalignment  $c$  for fixed separation  $\theta_2 = 10^{-3}$ . Other parameters are chosen as  $\bar{N} = 0.01$ ,  $m, n \leq 3$ .

### Appendix G: Comparison with the conventional method

To compare the conventional method with our method, we assume the centroid is  $\frac{1}{2}(\phi_1 + \phi_2) = 2\pi/3$  and choose the phase delay  $\delta = 0, \frac{\pi}{2}$ , which is conventionally used to extract information about the coherence function. We calculate the FI for the POVM with phase delay  $\delta = 0, \frac{\pi}{2}$ , corresponding to  $c = 2\pi/3, -\pi/3$ . The FI and QFI are shown in Fig. G3 as a function of separation. It is clear that when the separation  $\theta_2$  tends to zero, the FI vanishes, which implies the resolution limit, but the QFI remains a constant. This shows that a better POVM, such as the POVM we construct, can help avoid this limit.

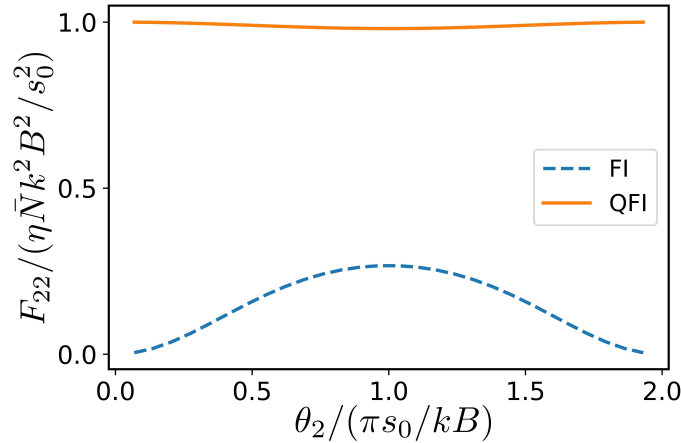


Figure G3: Approximate Fisher information (blue dashed curve) and the quantum Fisher information (solid orange curve) as a function of separation  $\theta_2$ . Other parameters are chosen as  $\bar{N} = 0.01$ ,  $m, n \leq 3$ .

We can read from Fig. G3 that the conventional method requires the separation to be comparable to  $s_0/kB$  to get reasonable sensitivity. This is consistent with the fact that the angular resolution of an interferometric array is approximately  $\lambda/B$ , where  $\lambda$  is the wavelength of the received state. As a practical example, we consider the case where the observation is made with wavelength  $\lambda = 5$  mm and longest baseline  $B = 10$  km. Then the resolution of the conventional method is  $\lambda/B = 5 \times 10^{-7}$  radians  $\approx 0.1''$ . For this case, when the angular separation of the two point sources is  $\theta_2/s_0 = 0.05''$  and  $\eta\bar{N} = 0.01$ , the Fisher information of our optimal measurement is larger than the conventional method by a factor of roughly 4. If we assume the mean square error of estimating the angular separation  $\theta_2/s_0$  scales with the number of samples  $n$  as  $\Delta(\theta_2/s_0)^2 \propto 1/n$ , this implies that our optimal measurement can shorten the observation time by a factor of 4 to achieve the same sensitivity. When the angular separation of the two point sources is  $\theta_2/s_0 = 0.01''$ , the Fisher information of our optimal measurement is larger than the conventional method by a factor of roughly 30, which shortens the observation time by a factor of 30. Finally, when the angular separation of the two point sources is  $0.005''$ , the Fisher information of our optimal measurement is larger than the conventional method by a factor of roughly 100, which shortens the observation time by a factor of 100.